Inorg. Chem. **2005**, *44*, 9185–9191

Crystal Structures, Raman Spectroscopy, and Magnetic Properties of $Ba_{7.5}Al_{13}Si_{29}$ and $Eu_{0.27}Ba_{7.22}Al_{13}Si_{29}$

Cathie L. Condron, Rhiannon Porter, Ting Guo, and Susan M. Kauzlarich*

Department of Chemistry, One Shields Avenue, University of California, Davis, California 95616

Received April 1, 2005

The framework-deficient clathrate phases $Ba_{7.5}Al_{13}Si_{29}$ and $Eu_{0.27}Ba_{7.22}Al_{13}Si_{29}$ were prepared using a molten Al flux. Single-crystal X-ray diffraction confirmed the two phases to be clathrate type I (space group $Pm\bar{3}n$). For $Eu_{0.27}Ba_{7.22}Al_{13}Si_{29}$, single-crystal X-ray diffraction revealed the Eu to partially occupy the 2a position. Microprobe analysis of single crystals provided the stoichiometry, and Raman spectroscopy was used to investigate the guest framework interactions. The Raman spectra are consistent with both $Ba_{7.5}Al_{13}Si_{29}$ and $Eu_{0.27}Ba_{7.22}Al_{13}Si_{29}$ having minimal guest–host interactions. Magnetic susceptibility data for $Eu_{0.27}Ba_{7.22}Al_{13}Si_{29}$ imply weak magnetic ordering and indicate a 2+ oxidation state for the Eu ion.

Introduction

Binary and ternary group-IV-containing clathrate phases provide an exciting area of research. These phases show rich crystal chemistry and display a wide variety of physical properties. One example is the discovery of superconductivity in the metal-doped clathrate phases Ba_xSi_{46}, and $Ba_xNa_ySi_{46}$.[1−4] Alternatively, they are potential candidates for band gap engineering based on group-IV elements because the guest-free clathrate structures such as Si_{34}, Si_{46}, Ge_{34}, and Ge_{46} have theoretically been shown to have a much larger band gap than the ground state of Si and Ge cubic and diamond phases.[5,6] In particular, ternary clathrate phases show excellent thermoelectric figures of merit and have the advantage of fine-tuning properties with subtle changes in composition.[7−9] Among the most studied clathrate phases for thermoelectric applications are the ternary phases $Sr_8Ga_{16}Ge_{30}$,[7,10−14] $Ba_8Ga_{16}Si_{30}$,[7,10] and $Ba_8Ga_{16}Ge_{30}$,[10,15,16] which have high electrical conductivity and glasslike thermal conductivity.

Clathrate compounds consist of covalently bonded framework atoms that encapsulate "rattling" guest atoms. Numerous binary and ternary clathrate compounds have been prepared. Among these are A_8B_{46} (A = Na, K, Rb, Ba; B = Si, Ge), $A_8B_8C_{38}$ (A = Na, K, Rb; B = Al, Ga, In; C = Si, Ge, Sn), and $A_8B_{16}C_{30}$ (A = Sr, Ba, Eu; B = Al, Ga, In; C = Si, Ge, Sn), which are summarized in microreviews by Mudryk et al.,[17] as well as Bobev et al.,[18] and extensively by Kovnir et al.[19] There are several clathrate structure types which are made up of framework cages (covalently bonded atoms) with cations (or anions) residing in the center of the cages.

Type I clathrate phases crystallize in the cubic space group $Pm\bar{3}n$. The framework is made up of two types of covalently

* To whom correspondence should be addressed.

(1) Kawaji, H.; Yamanaka, S.; Ishikawa, M. *Phys. Rev. B* **1995**, *74*, 1472.
(2) Yamanaka, S.; Horie, H. O.; Kawaji, H.; Ishikawa, M. *Eur. J. Solid State Inorg. Chem.* **1995**, *32*, 799.
(3) Kawaji, H.; Yamanaka, S.; Ishikawa, M. *Solid State Commun.* **1996**, *100*, 393.
(4) Yamanaka, S.; Enishi, E.; Fukuoka, H.; Yasukawa, M. *Inorg. Chem.* **2000**, *39*, 56.
(5) Gryko, J.; McMillan, P. F.; Marzke, R. F.; Ramachandran, G. K.; Patton, D.; Deb, S. K.; Sankey, O. F. *Phys. Rev. B* **2000**, *62*, R7707.
(6) A, K.; M, Y.; S, M. *Phys. Rev. B* **2001**, *64*, 045206.
(7) Cohn, J. L.; Nolas, G. S.; Fessatidis, V.; Metcalf, T. H.; Slack, G. A. *Phys. Rev. Lett.* **1999**, *82*, 779.
(8) Nolas, G. S. *Mater. Res. Soc. Symp. Proc.* **1999**, *545*, 435.
(9) Nolas, G. S.; Weakley, T. J. R.; Cohn, J. L.; Sharma, R. *Phys. Rev. B* **2000**, *61*, 3845.
(10) Blake, N. P.; Latturner, S.; Bryan, J. D.; Stucky, G. D.; Metiu, H. *J. Chem. Phys.* **2001**, *115*, 8060.
(11) Blake, N. P.; Mollnitz, L.; Kresse, G.; Metiu, H. *J. Chem. Phys.* **1999**, *111*, 3133.
(12) Chakoumakos, B. C.; Sales, B. C.; Mandrus, D. G.; Nolas, G. S. *J. Alloys Compd.* **2000**, *296*, 80.
(13) Keppens, V.; McGuire, M. A.; Teklu, A.; Laermans, C.; Sales, B. C.; Mandrus, D.; Chakoumakos, B. C. *Physica B* **2002**, *316−317*, 95.
(14) Nolas, G. S.; Cohn, J. L.; Slack, G. A.; Schujman, S. B. *Appl. Phys. Lett.* **1998**, *73*, 178.
(15) Bentien, A.; Christensen, M.; Bryan, J. D.; Sanchez, A.; Paschen, S.; Steglich, F.; Stucky, G. D.; Iversen, B. B. *Phys. Rev. B* **2004**, *69*, 045107/1.
(16) Bryan, J. D.; Blake, N. P.; Metiu, H.; Stucky, G. D.; Iversen, B. B.; Poulsen, R. D.; Bentien, A. *J. Appl. Phys.* **2002**, *92*, 7281.
(17) Mudryk, Y.; Rogl, P.; Paul, C.; Berger, S.; Bauer, E.; Hilscher, G.; Godart, C.; Noel, H.; Saccone, A.; Ferro, R. *Physica B* **2003**, *328*, 44.
(18) Bobev, S.; Sevov, S. C. *J. Solid State Chem.* **2000**, *153*, 92.
(19) Kovnir, K. A.; Zaikina, J. V.; Reshetova, L. N.; Olenev, A. V.; Dikarev, E. V.; Shevelkov, A. V. *Inorg. Chem.* **2004**, *43*, 3230.

10.1021/ic050483d CCC: $30.25
Published on Web 11/09/2005

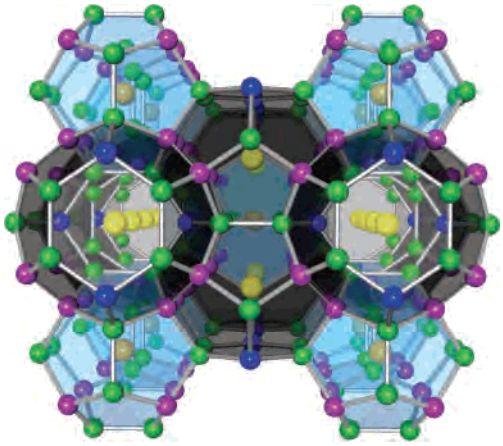

Figure 1. Polyhedral structure of the type I clathrate. Framework atoms are designated by color. The 6c sites are blue, the 16i sites are purple, and the 24k sites are green. The 2a Ba sites are orange, and the 6d Ba sites are yellow.

bonding polyhedral cages, two 20-member pentagonal dodecahedra, and six 24-member tetrakaidecahedra. The cubic structure can be constructed by connecting the tetrakaidecahedra by their faces to form infinite rods, which are themselves connected to form a cube of which the voids are filled by pentagonal dodecahedra. The unit cell of the type I clathrate structure is illustrated in Figure 1.

It is apparent that the properties exhibited by clathrate compounds depend strongly on the structural characteristics. For example, how strongly the guest atom is hybridized to the framework can increase or decrease the T_c in superconducting clathrate phases.[4,20−23] Alternatively, deviations from ideal stoichometries, which form vacancies, can change a p-type conductor to an n-type conductor, or effect the overall figure of merit of the compound, as demonstrated by Mudryk et al. with the solid solution $Eu_{2-x}(Sr, Ba)_{6-x}M_ySi_{46-y}$ (M = Al, Ga), [24] as well as by others with the Ge-containing clathrates.[14,16] The clathrate phases containing heavier framework elements have been well studied because of their thermoelectric applications. Stoichiometry is important for materials optimization, and the properties of type I clathrate phases are sensitive to subtle changes in composition.

This paper presents the single-crystal structure of two type I clathrate phases, $Ba_{7.5}Al_{13}Si_{29}$ and $Eu_{0.27}Ba_{7.22}Al_{13}Si_{29}$. Large single crystals of these phases can be prepared from an Al flux. Stoichiometry is determined by microprobe analysis. These compositions have not been investigated to date and the Al−Si-containing clathrates have not been studied in detail. Raman spectroscopy of the two phases and magnetic properties of $Eu_{0.27}Ba_{7.22}Al_{13}Si_{29}$ are presented and discussed.

Experimental Section

Synthesis. $Ba_{7.5}Al_{13}Si_{29}$ and $Eu_{0.27}Ba_{7.22}Al_{13}Si_{29}$ were synthesized from the elements Ba (Johnson Matthey, 99.9%), Eu (Ames Lab, 99.99%), Si (AESAR, 99.999%), and Al (Matheson Colemen and Bell 99.6%) using the high-temperature metallic solution growth method.[25] All preparations were performed in a nitrogen-filled drybox with water levels less than 1 ppm. Large single crystals (1−60 mg) of $Ba_{7.5}Al_{13}Si_{29}$ and $Eu_{0.27}Ba_{7.22}Al_{13}Si_{29}$ were grown using the ratio 2Ba:30Si:70Al and 2Eu:2Ba:30Si:70Al, respectively, and scaled to 1 g of Al. Larger single crystals can be prepared by increasing the volume of the reaction. The elements were layered into a 2 mL alumina crucible and placed into a fused silica tube. A second alumina crucible, filled with SiO_2 wool, was inverted and placed on top of the first. The fused silica tube was subsequently sealed under 0.2 atm of argon. The reaction vessel was heated from room temperature to 1000 °C in 4 h and slowly cooled at 0.6 °C/h to 900 °C, where it was removed from the furnace and the excess liquid was decanted. When the reactions were opened, large multifaceted single crystals coated in excess aluminum were discovered. The remaining aluminum was removed by soaking the crystals in an ∼5 M solution of NaOH until the crystal surfaces became clean. The crystals were then washed several times with water and acetone.

Microprobe Analysis. Single crystals of $Ba_{7.5}Al_{13}Si_{29}$ and $Eu_{0.27}Ba_{7.22}Al_{13}Si_{29}$ were obtained from several different reactions, mounted in epoxy, and polished for subsequent analysis. A Cameca SX-100 electron microprobe equipped with five wavelength-dispersive spectrometers, operating at 10 nA current with a 20 keV accelerating potential was used for analysis. Net elemental intensities for Al and Si were determined with respect to pure elemental calibration standards that were polished before the measurement to ensure the elements were not oxidized. $EuPO_4$ and $BaAl_{3.54}Si_{0.41}$ were used as standards to determine the net elemental intensities for Eu and Ba, respectively. Totals for all analyses were 100%. The elemental stoichiometries were quantitatively determined to be $Ba_{7.5(2)}Al_{13.0(1)}Si_{29.2(2)}$ and $Eu_{0.27(2)}Ba_{7.22(2)}Al_{13.3(1)}Si_{29.21(2)}$. The compositions were homogeneous within crystals and within standard deviation or identical when compared with crystals from different reactions.

Powder X-Ray Diffraction. X-ray powder diffraction data for $Ba_{7.5}Al_{13}Si_{29}$ were collected with an INEL CPS 120, which performs the simultaneous collection of diffracted X-rays over a 120° range in 2θ. X-rays (Cu Kα radiation) were generated with an XRG 3000 source operating at 30 kV and 30 mA. X-ray powder diffraction data for $Eu_{0.27}Ba_{7.22}Al_{13}Si_{29}$ were collected with a Sintag PAD-V employing Cu Kα radiation. Data acquisition for both phases was performed with WinAcq software. Sample analyses and Rietveld refinement of selected samples were performed using the REITICA software package. The peak profile was chosen to be pseudo-Voigt (Howard asymmetry), and the background was fit to a fifth-order polynomial. Atomic positions, as well as the overall temperature factors, were held constant.

Single-Crystal X-Ray Diffraction. The single-crystal X-ray diffraction data were collected at 90 K using a Bruker SMART 1000 CCD diffractometer employing graphite-monochromatized Mo Kα radiation (λ = 0.71069 Å). Data were collected in full sphere with 0.3° scans in ω and exposure time of 30 s per frame. Lorentz and polarization effects were corrected for using the SAINT program, and absorption corrections were based on fitting a function to the empirical transmission surface as sampled by multiple

(20) Fukuoka, H.; Kiyoto, J.; Yamanaka, S. *Inorg. Chem.* **2003**, *42*, 2933.
(21) Fukuoka, H.; Kiyoto, J.; Yamanaka, S. *J. Phys. Chem. Solids* **2004**, *65*, 333.
(22) Gat, I. M.; Fudamoto, Y.; Kinkhabwala, A.; Larkin, M. I.; Luke, G. M.; Merrin, J.; Nachumi, B.; Uemura, Y. J.; Kojima, K. M.; Eiji, E.; Yamanaka, S. *Physica B* **2000**, *289&290*, 385.
(23) Moriguchi, K.; Yonemura, M.; Shintani, A. *Phys. Rev. B* **2000**, *61*, 9859.
(24) Mudryk, Y.; Rogl, P.; Paul, C.; Berger, S.; Bauer, E.; Hilscher, G.; Godart, C.; Noel, H. *J. Phys.: Condens. Matter* **2002**, *14*, 7991.
(25) Canfield, P. C.; Fisk, Z. *Z. Philos. Mag. B* **1992**, *65*, 1117.

Table 1. Crystal Data and Structure Refinement for $Ba_{7.5}Al_{13}Si_{29}$ and $Eu_{0.27}Ba_{7.22}Al_{13}Si_{29}$

chemical formula[a]	$Ba_{7.5}Al_{13}Si_{29}$	$Eu_{0.27}Ba_{7.22}Al_{13}Si_{29}$
space group	*Pm*$\bar{3}$*n* (no. 223)	*Pm*$\bar{3}$*n* (no. 223)
a (Å)	10.6246 (12)	10.6306 (12)
V Å^3	1199.3 (2)	1201.4 (2)
Z	1	1
density (calcd)[a] Mg/m^3	3.047	3.057
density (measured) Mg/m^3	3.055	3.038
absorption coeff mm^{-1}	7.04	7.14
θ range	2.71−8.23°	2.71−8.06°
reflns collected	12 746	8791
independent reflns	294 [*R*(int) = 0.0424]	291 [*R*(int) = 0.0361]
data/restraints/params	294/0/18	291/0/18
GOF on F^2	1.210	1.274
final R indices [$I > 2\sigma(I)$][b]	R1 = 0.0136	R1 = 0.0145
	wR2 = 0.0248	wR2 = 0.0351
R indices (all data)	R1 = 0.0153	R1 = 0.0155
	wR2 = 0.0252	wR2 = 0.0356
extincion coeff	0.00221(15)	0.0037(3)
largest diff. peak and hole e·Å^{-3}	0.360 and −0.296	0.548 and −0.644

[a] Determined from microprobe analysis. [b] $R1 = [\sum||F_0| - |F_c||]/\sum|F_0|$; $wR2 = \{[\sum w[(F_0)^2 - (F_c)^2]^2]\}^{1/2}$; $w^{-1} = [\sigma^2(F_o)+(0.0471P)^2+(0.5945P)]$ where $P = [\max(F_o^2,0)+2F_c^{2/3}]$.

equivalent reflections (program SADABS).[26] The structure solution was obtained by direct methods and refined by full-matrix least-squares refinement against F_0^2 using the SHELXTL 6.10 package (see Table 1).[26]

Density Measurements. Archimedes principle was used to measure the densities of $Ba_{7.5}Al_{13}Si_{29}$ and $Eu_{0.27}Ba_{7.22}Al_{13}Si_{29}$ (given in Table 1). Methylene iodide (CH_2I_2, density of 3.310 g/mL at 23 °C) was used as a standard solution.

Raman Spectroscopy. Raman spectra were collected using a frequency-doubled Nd:YAG pumped laser. The central wavelength was 532 nm, and the bandwidth was ∼1.0 nm. The laser beam was first sent into a homemade inverted microscope equipped with a Raman filter (Omega Optical, 538AELP). The light was focused onto the sample by a microscope objective (Ziess Acroplan 0.8 NA 63×) after the Raman filter. The backscattered light from the sample was collected using the same objective. This light was then focused to a fiber, which coupled the light into a spectrometer (Acton, SpectraPro 300i), and was detected by a charge-coupled device (Roper Scientific, EEV CCD30). Spectral resolution was estimated at 15−20 cm^{-1}. The power at the sample was 10−15 mW, and the focal spot size was of the order 3 μm. Raman spectra were collected for 100 s of each acquisition, and the spectra were subsequently summed using WinSpec32 (Roper Scientific) to equal a 1000 s total acquisition time.

Magnetic Measurements. DC magnetization data were collected using a Quantum Design MPMS superconducting quantum interference device (SQUID) magnetometer with a 7 T superconducting magnet. Temperature- and field-dependent magnetization measurements of $Eu_{0.27}Ba_{7.22}Al_{13}Si_{29}$ were obtained by using a 0.02597 g clean, single crystal placed in a straw. The temperature-dependent data were obtained by measuring zero-field-cooled (ZFC) magnetization from 2 to 300 K and field-cooled (FC) magnetization from 2 to 300 K in an applied magnetic field of 100 Oe. Field-dependent magnetization data were taken at 10 K by sweeping though fields from 0 to +6 T and +6 to 0 T

Results and Discussion

Throughout the literature, ternary group IV clathrate phases have been prepared mainly by direct reaction of the elements to produce powder and polycrystalline materials. Because most clathrate phases exhibit cubic symmetry, anisotropic effects are not expected. Thus, for properties measurements such as Seebeck coefficient, resistivity, and thermopower, powder or polycrystalline samples are sufficient. However, thermal motion and disorder in thermoelectric clathrate phases are important factors in determining if and why clathrate phases exhibit good thermoelectric properties. This is especially true when considering the "phonon glass and electron crystal model" (PGEC). To explore these properties in detail, high-quality single-crystal neutron or synchrotron data are required. Additionally, for magnetization studies on phases that do not have magnetic ions, a sufficient sample size is required in order to get an adequate SQUID response. Thus, the flux method provides a fast and convenient approach of preparing high-quality single crystals of type I clathrate phases.

Using the flux method, several groups have prepared good-quality single crystals of clathrate phases containing the heavier framework elements, such as $Eu_4Ga_8Ge_{16}$, $Ba_8Ga_{16}Ge_{16}$, $Ba_8Ga_{16}Si_{16}$, and $Sr_8Ga_{16}Ge_{16}$.[27−30] Single-phase samples of $Ba_8Al_xSi_{42-3/4x}\square_{4-1/4x}$ where $x = 8$, 12, and 16 have been prepared by arc melting and annealing.[24] The formula $Ba_8Al_xSi_{42-3/4x}\square_{4-1/4x}$ was proposed assuming that these phases must be electron precise and assumes that the framework defects, in addition to Al substitution, provide charge compensation. $Ba_8Al_{16}Si_{30}$ and $Ba_8Al_{12}Si_{33}$ were reported to melt incongruently, Seebeck, resistivity, and thermal conductivity have been reported for $Ba_8Al_{16}Si_{30}$.[24] Lattice parameters for $Ba_8Al_xSi_{42-3/4x}\square_{4-1/4x}$ ($x = 8$, 12, 16) have been reported and increase with increasing Al content or decreasing Si content. Powder samples of $Ba_8Al_{16}Si_{30}$ were first prepared by Eisenmann, Schäfer, and Zagler,[31] who reported lattice parameters and elemental analyses. Syntheses of clathrate type I phases of the composition $Ba_{7.5}Al_{13}Si_{29}$ and $Eu_{0.27}Ba_{7.22}Al_{13}Si_{29}$ have not been reported and high-quality, large single crystals have not yet been reported for any clathrate phases of the Al−Si family.

$Eu_{0.27}Ba_{7.22}Al_{13}Si_{29}$ is a new addition to the solid solution $Eu_2Ba_6Al_xSi_{36-x}$ first characterized by Mudryk et al.[24] Polycrystalline samples of $Eu_2Ba_6Al_8Si_{36}$ made by arc melting and annealing have been prepared, with reported lattice parameters of 10.4951(2) Å,[17,24] much smaller than the lattice parameter for $Eu_{0.27}Ba_{7.22}Al_{13}Si_{29}$, at 10.6306(12) Å. However, since there is a greater amount of Al in $Eu_{0.27}Ba_{7.22}Al_{13}Si_{29}$, this is expected and consistent with previously reported examples, as mentioned above.[17,24]

(26) Sheldrick, G. M. *XRD Single-Crystal Software*; Bruker Analytical X-ray Systems: Madison, WI, 1999.

(27) Christensen, M.; Bryan, J. D.; Birkedal, H.; Stucky, G. D.; Lebech, B.; Iversen, B. B. *Phys. Rev. B* **2003**, *68*, 174428/1.

(28) Latturner, S. E.; Bryan, J. D.; Blake, N.; Metiu, H.; Stucky, G. D. *Inorg. Chem.* **2002**, *41*, 3956.

(29) Bryan, J. D.; Srdanov, V. I.; Stucky, G. D. Synthesis and physical properties of alkali earth metal encapsulated germanium clathrate compounds. In *Book of Abstracts, 217th ACS National Meeting, Anaheim, Calif., March 21−25*; American Chemical Society: Washington, DC, 1999; p 637.

(30) Bentien, A.; Palmqvist, A. E. C.; Bryan, J. D.; Latturner, S.; Stucky, G. D.; Furenlid, L.; Iversen, B. B. *Angew. Chem.* **2000**, *39*, 3613.

(31) Eisenmann, B.; Schaefer, H.; Zagler, R. *J. Less-Common Met.* **1986**, *118*, 43.

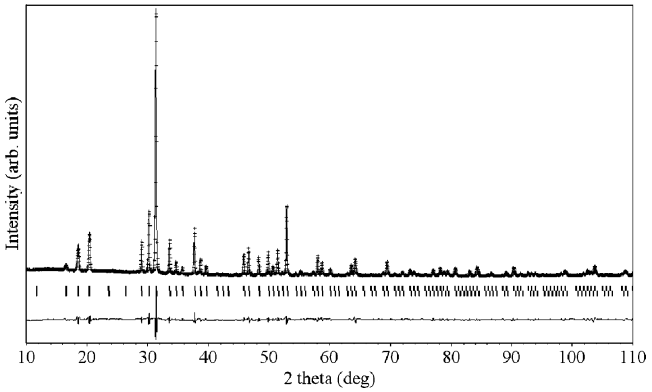

Figure 2. Rietveld profile fit for $Ba_{7.5}Al_{13}Si_{29}$. Experimental data points are shown as black circles, and the theoretical fit is shown as a gray solid curve. The data were refined for the space group $Pm\bar{3}n$ (black ticks), and the difference between the observed and theoretical patterns is shown below the black ticks. $a = 10.6373(11)$ Å, $R_p = 4.03\%$, $R_{wp} = 5.46\%$, $R_{Bragg} = 6.30\%$.

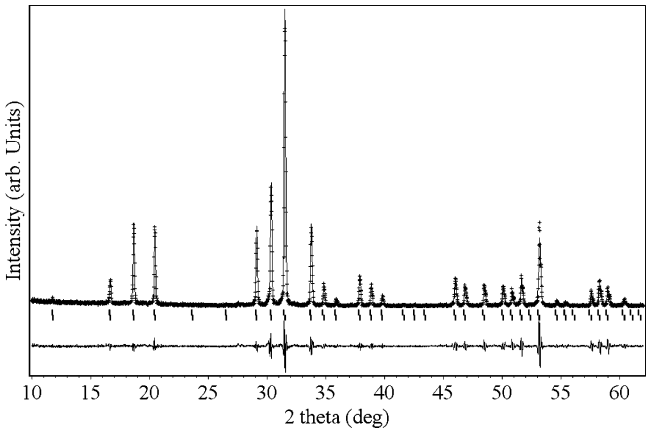

Figure 3. Rietveld profile fit for $Eu_{0.27}Ba_{7.22}Al_{13}Si_{29}$. Experimental data points are shown as black circles, and the theoretical fit is shown as a gray solid curve. The data were refined for the space group $Pm\bar{3}n$ (black ticks), and the difference between the observed and theoretical patterns is shown below the black ticks. $a = 10.631(10)$ Å, $R_p = 3.00\%$, $R_{wp} = 13.30\%$, $R_{Bragg} = 4.50\%$.

Powder X-ray diffraction experiments were used to determine phase purity, as well as room-temperature lattice parameters. Several clean crystals were selected and ground into a sufficient particle size for powder X-ray diffraction analysis. Figures 2 and 3 show the Rietveld profile fits for $Ba_{7.5}Al_{13}Si_{29}$ and $Eu_{0.27}Ba_{7.22}Al_{13}Si_{29}$, respectively. It is clear from the diffraction patterns and corresponding fits that there were no obvious impurities in the $Ba_{7.5}Al_{13}Si_{29}$ and $Eu_{0.27}Ba_{7.22}Al_{13}Si_{29}$ samples. The Rietveld refinement of $Ba_{7.5}Al_{13}Si_{29}$ yielded $a = 10.6373(11)$ Å, $R_p = 4.03\%$, $R_{wp} = 5.46\%$, and $R_{Bragg} = 6.30\%$. The unit cell edge is slightly larger than that found from single-crystal X-ray diffraction ($a = 10.6246(12)$ Å) performed at 90 K, as is expected for a higher-temperature measurement. Similarly, the Rietveld refinement of $Eu_{0.27}Ba_{7.22}Al_{13}Si_{29}$ yielded $a = 10.631(10)$ Å, $R_p = 3.00\%$, $R_{wp} = 13.30\%$, and $R_{Bragg} = 4.50\%$.

Single-crystal X-ray diffraction studies confirmed that $Ba_{7.5}Al_{13}Si_{29}$ and $Eu_{0.27}Ba_{7.22}Al_{13}Si_{29}$ crystallize in the cubic space group $Pm\bar{3}n$ with unit cell edges of 10.6246(12) and 10.6306(12) Å, respectively. The unit cell edge of $Ba_{7.5}Al_{13}Si_{29}$ is slightly larger than that of $Ba_8Al_{16}Si_{30}$ reported by Eisenmann, Schäfer, and Ziegler at 10.6068(30) Å and by Mudryk at 10.6285 Å.[24,31] However, only lattice parameters determined from powder X-ray diffraction were reported. The observed deviations in the lattice parameters of this work versus values previously published are presumably the result of different stoichometries and the data collection temperature for the crystals. Our stoichiometry is determined from microprobe analysis of several single crystals, while their stoichiometry was assigned on the basis of the Al/Ge and Ga/Si ratios of the analogous compounds $Ba_8Al_{16}Ge_{30}$ and $Ba_8Ga_{16}Si_{30}$, respectively, determined by Laue diffraction characterization.[24,31] Our lattice parameters are consistent with the trend mentioned previously, where the lattice parameters increase with increasing amount of Al or decreasing amount of Si.

Table 2. Atomic Coordinates and Equivalent Isotropic Displacement Parameters (U_{eq})[a] for $Ba_{7.5}Al_{13}Si_{29}$ and $Eu_{0.27}Ba_{7.22}Al_{13}Si_{29}$

atom	site	x	y	z	U_{eq} (Å^2)	occupancy
			$Ba_{7.5}Al_{13}Si_{29}$			
Ba(1)	2a	0	0	0	0.00573(17)	0.924(4)
Ba(2)	6d	0	0.25000	0.50000	0.02015(14)	0.924(3)
M(1)	6c	0.25000	0	0.50000	0.0098(3)	0.913
M(2)	16i	0.18515(5)	0.18515(5)	0.18515(5)	0.0082(2)	0.913
M(3)	24k	0.11809(7)	0	0.30554(7)	0.0071(2)	0.913
			$Eu_{0.27}Ba_{7.22}Al_{13}Si_{29}$			
Ba/Eu(1)	2a	0	0	0	0.0066(2)	0.86(2)/0.09(2)
Ba(2)	6d	0	0.25000	0.50000	0.01789(17)	0.922(4)
M(1)	6c	0.25000	0	0.50000	0.0089(4)	0.913
M(2)	16i	0.18489(6)	0.18489(6)	0.18489(6)	0.0083(3)	0.913
M(3)	24k	0.11735(8)	0	0.30521(8)	0.0072(2)	0.913

[a] U_{eq} is defined as one-third of the trace of the orthogonalized U^{ij} tensor.

There are three crystallographically distinct framework sites in the clathrate type I structure, which are listed in Table 2. Each site is tetrahedrally coordinated to four other framework atoms and is distorted from an ideal tetrahedral environment by different degrees. The degree of distortion in the local environments of each framework site plays a key role in understanding the structure and how it affects the properties. Previous studies suggest the 6c site is preferentially filled by groups 12 and 13, as well as transition metal framework elements.[32−34] This is indeed the case reported for $Ba_8Ga_{16}Si_{30}$,[31] where the majority of the gallium is located in the 6c and 16i sites. Eisenmann also suggests that the 6c site is completely filled by Al in $Ba_{7.5}Al_{16}Ge_{30}$. Because the electron densities, and thus the scattering power, of Al and Si are very similar, it was not possible to distinguish between them during refinement of the X-ray data of $Ba_{7.5}Al_{13}Si_{29}$ and $Eu_{0.27}Ba_{7.22}Al_{13}Si_{29}$. Mudryk et al. assigned the Al to the 6d position on the basis of bond length analysis for the stoichiometry $Eu_2Ba_6Al_8Si_{36}$. In our case, the framework bond lengths are not significantly different from each other, and therefore, no distinction between Al and Si could be assumed. In addition, when the structure was refined with no constraints, it became apparent that the sites were not fully occupied and the refinement with either

(32) Latturner, S. E.; Bryan, D.; Blake, N.; Metiu, H.; Stucky, G. D. *Inorg. Chem.* **2002**, 41.
(33) Kuhl, B.; Czybulka, A.; Schuster, H.-U. *Z. Anorg. Allg. Chem.* **1995**, *621*, 1.
(34) Cordier, G.; Woll, P. *J. Less-Common Met.* **1991**, *169*, 291.

all Al or all Si in the framework sites resulted in similar refinement parameters, R1, wR2, and GOF. For this reason, the structure was modeled according to the stoichiometry provided by microprobe analysis, which suggests defects within the structure and cannot be rationalized within the model proposed by Murdyk et al.[24] This was done by setting the site occupancy factor of every framework site to 0.913 instead of 1 and letting each framework site share equal amounts of Si and Al, giving a total of 13 Al and 29 Si. Using this model, the Ba and Ba/Eu occupancies were allowed to refine in $Ba_{7.5}Al_{13}Si_{29}$ and $Eu_{0.27}Ba_{7.22}Al_{13}Si_{29}$, respectively. The refinement of $Ba_{7.5}Al_{13}Si_{29}$ yielded a total of 7.39 Ba, slightly less than the amount found from microprobe analysis, but within standard deviation. The Eu/Ba occupancies $Eu_{0.27}Ba_{7.22}Al_{13}Si_{29}$ refined to 0.18 Eu and 7.27 Ba and are different from the stoichiometry given by microprobe analysis. Experimental density measurements, however, are in good agreement with the stoichiometry determined from microprobe data. Therefore, the stoichiometries obtained from microprobe data are used throughout. Table 2 lists the position, occupancy, and isotropic displacement parameters for $Ba_{7.5}Al_{13}Si_{29}$ and $Eu_{0.27}Ba_{7.22}Al_{13}Si_{29}$. Further structural studies are underway, including neutron diffraction and NMR, to provide insight into the site specificity of Al in these Al−Si clathrate phases.

It is interesting, but not surprising, that both $Ba_{7.5}Al_{13}Si_{29}$ and $Eu_{0.27}Ba_{7.22}Al_{13}Si_{29}$ do not obey the Zintl rule. It has been shown that for clathrate silicides there is no need for strict correspondence between the framework composition and the number of electrons donated by the guest cation.[35−38] This is perhaps best illustrated in the binary silicide clathrates Ba_xSi_{46} which exhibit an increasing superconducting T_c as the Ba content increases.[39−42] Another example is $Rb_{8-x}Si_{46}$ ($x < 2$), which exhibits metallic conductivity and Pauli paramagnetism typical of metals.[43]

Raman scattering spectra of $Ba_{7.5}Al_{13}Si_{29}$ and $Eu_{0.27}Ba_{7.22}Al_{13}Si_{29}$ are shown in Figure 4. $Ba_{7.5}Al_{13}Si_{29}$ exhibits a strong peak at 516 cm^{-1} and a broad peak centered around 200−400 cm^{-1} that may be made up of poorly resolved stretches. Similarly, $Eu_{0.27}Ba_{7.22}Al_{13}Si_{29}$ exhibits a strong peak at 507 cm^{-1} and a broad envelope centered around 200−400 cm^{-1}. In addition, the $Eu_{0.27}Ba_{7.22}Al_{13}Si_{29}$ spectrum shows a small sharp peak at 166 cm^{-1}. In both of $Ba_{7.5}Al_{13}Si_{29}$ and $Eu_{0.27}Ba_{7.22}Al_{13}Si_{29}$, the highest-frequency peak (516 and 507 cm^{-1}, respectively) is very strong. The smaller peaks at lower frequencies are smeared out and cannot be individually identified.

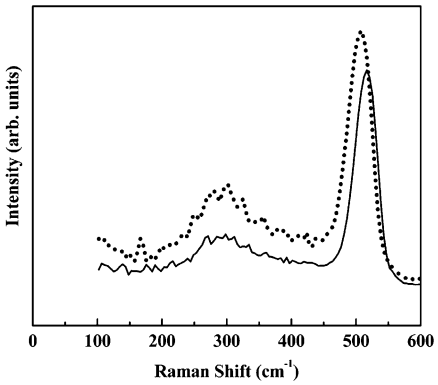

Figure 4. Raman spectra of $Ba_{7.5}Al_{13}Si_{29}$ (solid line) and $Eu_{0.27}Ba_{7.22}Al_{13}Si_{29}$ (dotted line).

As pointed out by Shimizu et al.[44] there are three key points to consider when examining Raman spectra of clathrate phases: (1) the low-frequency vibrational bands associated with the rattling guest atoms, (2) the lowest-frequency framework band (which exhibits a softening in frequency under pressure),[40,44,45] and (3) the highest-frequency framework band, which can be used to gauge how strongly the guest atoms are interacting with the framework. For our comparison, we will concentrate on point 3.

The large Raman peak at about 430−461 cm^{-1} has been observed in the type I clathrate phases, Ba_8Si_{46}, K_8Si_{46}, and $I_8Si_{44}I_2$, and has been assigned to the highest-frequency framework mode.[44] The all-Si mode exhibited in Ba_8Si_{46} has a lower energy (438 cm^{-1}) compared with the Al−Si framework vibrations of $Ba_8Al_{13}Si_{29}$ and $Eu_{0.27}Ba_{7.22}Al_{13}Si_{29}$ (517 and 508 cm^{-1}, respectively). Therefore, this strong peak in $Ba_{7.5}Al_{13}Si_{29}$ and $Eu_{0.27}Ba_{7.22}Al_{13}Si_{29}$ is assigned to the corresponding Al−Si framework vibrations. The possible reasons for the increased vibrational frequencies compared with Ba_8Si_{46} include the reduced mass by replacing Si with Al, changes in bond strength (Si−Si and Si−Al) as a result of the structural changes upon insertion of Al into the Si network, defects in the structure, and weakened guest−host interactions by replacing Si with Al. When comparing the changes in bond lengths between $Ba_{7.5}Al_{13}Si_{29}$ and $Eu_{0.27}Ba_{7.22}Al_{13}Si_{29}$ with respect to Ba_8Si_{46}, we see a lengthening of bonds ranging from 1 to −5%. Bond lengths for Ba_8Si_{46} were taken for qualitative comparison from data reported by Yamanaka et al.[4] In both $Ba_{7.5}Al_{13}Si_{29}$ and $Eu_{0.27}Ba_{7.22}Al_{13}Si_{29}$, the M(2)−M(2) and M(1)−M(3) bonds were affected the greatest, 4.73(1)% and 3.27(1)%, respectively, for $Ba_{7.5}Al_{13}Si_{29}$ and 5.17(1)% and 3.6(1)%, respectively, for $Eu_{0.27}Ba_{7.22}Al_{13}Si_{29}$. The lengthening of the M(2)−M(2) and M(1)−M(3) bonds support the increase in vibrational frequencies as a result of bond strength and structural changes associated with the addition of Al into the Si framework.

(35) Ramachandran, G. K.; McMillan, P. F.; Diefenbacher, J.; Gryko, J.; Dong, J.; Sankey, O. F. *Phys. Rev. B* **1999**, *60*, 12294.
(36) Cros, C.; Pouchard, M.; Hagenmuller, P. *J. Solid State Chem.* **1970**, *2*, 570.
(37) Mingos, D., *Essential Trends in Inorganic Chemistry*; Oxford University Press: Oxford, 1998.
(38) Ramachandran, G. K.; McMillan, P. F.; Deb, S. K.; Somayazulu, M.; Gryko, J.; Dong, J.; Sankey, O. F. *J. Phys.: Condens. Matter* **2000**, *12*, 4013.
(39) Kume, T.; Fukuoka, H.; Koda, T.; Sasaki, S.; Shimizu, F.; Tse, J. *Phys. Rev. B* **2004**, *70*, 052101.
(40) Kume, T.; Fukuoka, H.; Koda, T.; Sasaki, S.; Shimizu, H.; Yamanaka, S. *Phys. Rev. Lett. 90*, 155503.
(41) Tse, J.; Desgreniers, S.; Li, Z.-q.; Ferguson, M.; Kawazoe, Y. *Phys. Rev. Lett.* **2002**, *89*, 195507.
(42) Melinon, P.; Keghelian, P.; Perez, A.; Champagnon, B.; Guyot, Y.; Saviot, L.; Reny, E.; Cros, C.; Pouchard, M.; Dianoux, A. J. *Phys. Rev. B* **1999**, *59*, 10099.
(43) Ramachandran, G. K.; McMillan, P. F.; Dong, J.; Sankey, O. F. *J. Solid State Chem.* **2000**, *154*, 626.
(44) Shimizu, H.; Kume, T.; Kuroda, T.; Sasaki, S.; Fukuoka, H.; Yamanaka, S. *Phys. Rev. B* **2003**, *68*, 212102.
(45) Kume, T.; Koda, T.; Sasaki, S.; Shimizu, H.; Tse, J. *Phys. Rev. B* **2004**, *70*, 052101.

Table 3. Bond Lengths (Å) and Angles (deg) for $Ba_{7.5}Al_{13}Si_{29}$ and $Eu_{0.27}Ba_{7.22}Al_{13}Si_{29}$

bond lengths		bond angles	
	$Ba_{7.5}Al_{13}Si_{29}$		
Ba(1)−M(2)	3.4073(9)	M(2)−M(3)−M(1)	105.58(3)
Ba(1)−M(3)	3.4802(9)	M(2)−M(3)−M(2)	106.68(3)
Ba(2)−M(1)	3.7564(4)	M(2)−M(3)−M(3)	106.89(2)
Ba(2)−M(3)	3.5914(6)	M(2)−M(2)−M(3)	109.25(2)
M(1)−M(3)	2.4966(8)	M(3)−M(2)−M(3)	109.69(2)
M(2)−M(2)	2.3866(17)	M(3)−M(1)−M(3)	108.37(2)
M(2)−M(3)	2.4522(6)	M(3)−M(1)−M(3)	111.70(3)
M(3)−M(3)	2.5093(15)	M(1)−M(3)−M(3)	124.15(2)
	$Eu_{0.27}Ba_{7.22}Al_{13}Si_{29}$		
Ba/Eu(1)−M(2)	3.4044(11)	M(2)−M(3)−M(1)	105.44(3)
Ba/Eu(1)−M(3)	3.4767(9)	M(2)−M(3)−M(2)	106.54(4)
Ba(2)−M(1)	3.7585(4)	M(2)−M(3)−M(3)	107.02(2)
Ba(2)−M(3)	3.5927(4)	M(2)−M(2)−M(3)	109.31(3)
M(1)−M(3)	2.5053(9)	M(3)−M(2)−M(3)	109.63(3)
M(2)−M(2)	2.398(2)	M(3)−M(1)−M(3)	108.47(2)
M(2)−M(3)	2.4525(7)	M(3)−M(1)−M(3)	111.49(4)
M(3)−M(3)	2.4951(17)	M(1)−M(3)−M(3)	124.254(19)

The highest-frequency framework mode has been shown to be sensitive to the degree of hybridization between the framework atoms and the guest atoms.[23,41,42] The intensity is diminished for the superconducting Ba_8Si_{46} phase and is strong for the $I_8Si_{44}I_2$ phase, reflective of the strong guest−host interaction found in Ba_8Si_{46} and relatively weak guest host interactions in $I_8Si_{44}I_2$. Thus, the strong bands at 516 and 507 cm^{-1} found for $Ba_{7.5}Al_{13}Si_{29}$ and $Eu_{0.27}Ba_{7.22}Al_{13}Si_{29}$, respectively, indicate that the guest−host interaction is weak compared to Ba_8Si_{46}. The participation of Eu in the guest−host framework interaction may be the reason $Eu_{0.27}Ba_{7.22}Al_{13}Si_{29}$ exhibits a reduced Raman frequency of 507 cm^{-1} as compared to $Ba_{7.5}Al_{13}Si_{29}$.

This hypothesis is also consistent with the broad stretch around 200−400 cm^{-1} found in both $Ba_{7.5}Al_{13}Si_{29}$ and $Eu_{0.27}Ba_{7.22}Al_{13}Si_{29}$. Bands are assigned by Shimizu et al. for Ba_8Si_{46}, K_8Si_{46}, and $I_8Si_{44}I_2$ to be the lowest-frequency framework vibrations. $I_8Si_{44}I_2$ shows a similarly broad, poorly resolved region similar to those observed in Figure 4. The combination of a strong, well-resolved band at about 510 cm^{-1} and poorly resolved broad bands at 200−400 cm^{-1} for the Ba and Eu/Ba phases is most consistent with weak guest−host framework interactions. Similar features are also observed for the $Ba_8Ga_{10}Si_{36}$ and $Ba_8Ga_{16}Si_{30}$ type I clathrate phases.[46] The acoustic vibrational modes associated with the rattling of the guest atoms inside the cages of $Ba_{7.5}Al_{13}Si_{29}$ and $Eu_{0.27}Ba_{7.22}Al_{13}Si_{29}$ should be present at lower frequencies than can be observed by our current method. The exception is the peak at 166.46 cm^{-1} observed in the $Eu_{0.27}Ba_{7.22}Al_{13}Si_{29}$ spectrum, which is reproducible under various conditions and between samples. This peak may be related to the vibrational modes produced by the motions of Eu and Ba atoms accommodated in the smaller cages (2a site) of $Eu_{0.27}Ba_{7.22}Al_{13}Si_{29}$.

Figure 5a shows the magnetic susceptibility and inverse susceptibility (inset) and Figure 5b shows the susceptibility times temperature and an inflated region of the susceptibility times temperature (inset) as a function of temperature at an applied field of 100 Oe for $Eu_{0.27}Ba_{7.22}Al_{13}Si_{29}$. $Eu_{0.27}Ba_{7.22}Al_{13}Si_{29}$ shows Curie−Weiss behavior over the entire temperature range. Hence, the experimental data were fit according to the Curie−Weiss law $\chi = C(T - \theta)^{-1}$, where C is the Curie constant, θ is the Weiss constant, and T is temperature. From least-squares analysis, C and θ were found to be 2.32 (2) and 3.46(2) K, respectively. The experimental moment obtained from the Curie constant via the equation $\mu_{exp} = (7.99C)^{1/2}$ was found to be 4.31(1) μ_B. The experimental moment is in good agreement with the calculated spin-only effective moment of 4.12(1) μ_B corresponding to 0.27 Eu, when considering Eu to be 2+ ($\mu_{eff} = 2[S(S+1)]^{1/2}$, for 0.27 Eu; $\mu = (0.27\mu_{eff}^2)^{1/2}$). The susceptibility times temperature as a function of temperature is temperature independent over most of the temperature range, with a sharp increase after 10 K, which is indicative of weak ferromagnetic coupling.

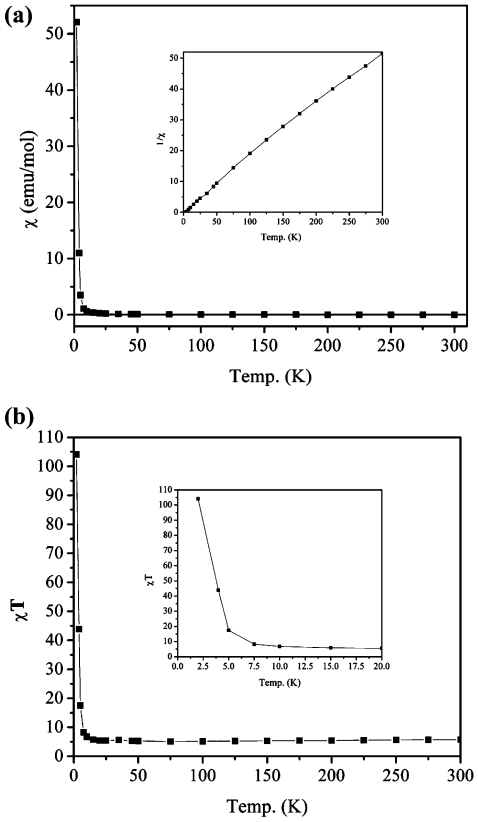

Figure 5. **(a)** Magnetic susceptibility (χ), (inset) inverse susceptibility ($1/\chi$) verses temperature, **(b)** susceptibility times temperature versus temperature at 100 Oe, and (inset) enlarged susceptibility times temperature versus temperature for $Eu_{0.27}Ba_{7.22}Al_{13}Si_{29}$.

Figure 6 shows the isothermal magnetization curve as a function of field at several temperatures. At 2 K, the sample shows spontaneous magnetization up to 6 T. The isothermal magnetization curves at 25 K and higher are linear with field, indicative of a paramagnetic state, and the magnetization is small compared to that at 10 K. This, along with a positive paramagnetic Curie constant, as well as the sharp increase in the susceptibility times temperature versus temperature after 10 K, suggests very weak ferro- or ferrimagnetic coupling is present in $Eu_{0.27}Ba_{7.22}Al_{13}Si_{29}$. There is no observable hysteresis in the magnetization upon cycling the

(46) Nataraj, D.; Nagao, J. *J. Solid State Chem.* **2004**, *177*, 1905.

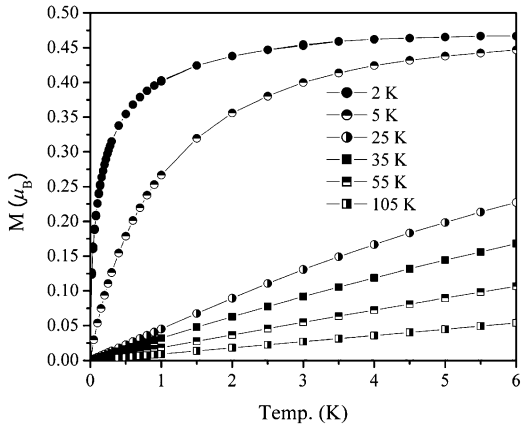

Figure 6. Isothermal magnetization curve as a function of field at several temperatures for $Eu_{0.27}Ba_{7.22}Al_{13}Si_{29}$.

magnetic field between 0 and 6 T at 2 or 5 K, implying $Eu_{0.27}Ba_{7.22}Al_{13}Si_{29}$ is a soft ferromagnet. The saturation moment of about 0.45 μ_B (1.89 μ_B expected) is less than expected for ferromagnetic ordering and suggests ferrimagnetic coupling of the Eu. $Eu_2Ba_6Al_8Si_{36}$ shows ferromagnetic type ordering at 32 K and also shows a lower-than-expected saturation moment of 5.5 μ_B per Eu (7 μ_B expected).[17] Decreasing the number of Eu in the structure should decrease the ferromagnetic ordering temperature, as is observed for $Eu_{0.27}Ba_{7.22}Al_{13}Si_{29}$.

Summary

Single crystals of $Ba_{7.5}Al_{13}Si_{29}$ and $Eu_{0.27}Ba_{7.22}Al_{13}Si_{29}$ were synthesized using the molten flux technique. It is possible that varying flux composition may provide compositional tuning for further investigation. Single-crystal X-ray diffraction confirmed the two phases to be clathrate type I (space group $Pm\bar{3}n$). Stoichiometry was determined from microprobe data and is consistent with the experimental density. For $Eu_{0.27}Ba_{7.22}Al_{13}Si_{29}$, single-crystal X-ray diffraction revealed the Eu to reside in the 2a position. Powder X-ray diffraction confirmed the lattice parameters and phase purity of both phases. Raman spectroscopy revealed a large peak at 517 and 508 cm^{-1} for $Ba_{7.5}Al_{13}Si_{29}$ and $Eu_{0.27}Ba_{7.22}Al_{13}Si_{29}$, respectively, and a broad band from 200 to 400 cm^{-1}, implying that the guest framework interactions are weak. Magnetic data are also consistent with stoichiometry, indicate a 2+ state for the Eu ions for $Eu_{0.27}Ba_{7.22}Al_{13}Si_{29}$, and show weak ferromagnetic-type ordering at low temperatures.

Acknowledgment. This research was sponsored by NSF (DMR-0120990) and the Jet Propulsion Laboratory. The authors are grateful to Sara Roeske for assistance with microprobe analysis and Håkon Hope, Peter Klavins, and Zachary Fisk for useful discussion.

Note Added after ASAP Publication. The Supporting Information Available paragraph was not present in the version published ASAP November 9, 2005; the corrected version was published November 21, 2005.

Supporting Information Available: Crystallographic data in cif format. This material is available free of charge via the Internet at http://pubs.acs.org.

IC050483D